ACS APPLIED MATERIALS & INTERFACES

www.acsami.org

Research Article

Large Low-Field Magnetoresistance (LFMR) Effect in Free-Standing $La_{0.7}Sr_{0.3}MnO_3$ Films

Cheng Zhang, Shuaishuai Ding, Kaiming Qiao, Jia Li, Zhe Li, Zhuo Yin, Jirong Sun, Jing Wang,* Tongyun Zhao, Fengxia Hu,* and Baogen Shen*

Cite This: *ACS Appl. Mater. Interfaces* 2021, 13, 28442−28450

Read Online

ACCESS | Metrics & More | Article Recommendations | Supporting Information

ABSTRACT: The realization of a large low-field magnetoresistance (LFMR) effect in free-standing magnetic oxide films is a crucial goal toward promoting the development of flexible, low power consumption, and nonvolatile memory devices for information storage. $La_{0.7}Sr_{0.3}MnO_3$ (LSMO) is an ideal material for spintronic devices due to its excellent magnetic and electronic properties. However, it is difficult to achieve both a large LFMR effect and high flexibility in LSMO films due to the lack of research on LFMR-related mechanisms and the strict LSMO growth conditions, which require rigid substrates. Here, we induced a large LFMR effect in an LSMO/mica heterostructure by utilizing a disorder-related spin-polarized tunneling effect and developed a simple transfer method to obtain free-standing LSMO films for the first time. Electrical and magnetic characterizations of these free-standing LSMO films revealed that all of the principal properties of LSMO were sustained under compressive and tensile conditions. Notably, the magnetoresistance of the processed LSMO film reached up to 16% under an ultrasmall magnetic field (0.1 T), which is 80 times that of a traditional LSMO film. As a demonstration, a stable nonvolatile multivalue storage function in flexible LSMO films was successfully achieved. Our work may pave the way for future wearable resistive memory device applications.

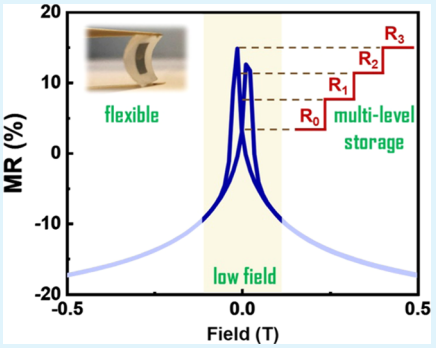

KEYWORDS: *$La_{0.7}Sr_{0.3}MnO_3$, mica, flexible device, LFMR, free-standing*

INTRODUCTION

Achieving a simple structure, low power consumption, and nonvolatility has always been a goal in the development of magnetic response oxide memory. Moreover, the development of flexible electronic devices also creates new demands for oxides.[1−8] Therefore, finding a material with both flexible and stable storage functions has become a hot topic in the field of oxides. Among the numerous oxides, lanthanum manganite perovskites, such as $La_{0.7}Sr_{0.3}MnO_3$ (LSMO), have shown great promise due to their complex magnetic and electrical transport properties. Compared to its counterparts, the strong ferromagnetic properties, very large magnetoresistance (MR), and high conductivity of LSMO make it more suitable for spintronic device research and fabrication.[9,10] Moreover, as a half-metallic perovskite manganite with near 100% spin polarization,[11] LSMO has attracted a large amount of attention in both theoretical and practical fields.[12,13] In particular, the high curie temperature, $T_c \sim 369$ K, of LSMO[14] and colossal magnetoresistance (CMR) property[15] have attracted much attention for potential applications in magnetic field sensing. However, practical applications regarding the CMR effect have been restricted by the required specific temperature (near T_c) and high magnetic fields (several tesla), and the MR is reduced to almost zero in low-temperature zones.[16,17] In addition, the deposition of LSMO films often relies on rigid substrates, limiting its potential for application in integrated flexible circuits. Therefore, the goal of combining low-field large MR effects and flexibility presents new challenges in this field.

Many methods, including fabricating artificial grain boundaries and interface phases and introducing a secondary phase (nonmagnetic or antiferromagnetic insulators), have been attempted to improve the extrinsic low-field magnetoresistance (LFMR) effects ($H \leq 1$ T) in manganites.[18−23] By utilizing the spin-polarized tunneling effect at the grain boundaries (GBs) and phase boundaries (PBs) of manganites, these studies amplify the LFMR effect with low energy consumption and further deepen the understanding of the CMR effect,[23−25] which further promotes the application of the LFMR effect such as magnetic tunnel junctions (MTJs) and magnetic storage devices.[26−28] On the other hand, to achieve a balance between flexibility and high quality, mica substrates with high temperature resistance (over 1000 °C) have been introduced in the deposition process for several

Received: February 26, 2021
Accepted: May 30, 2021
Published: June 9, 2021

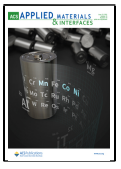

https://doi.org/10.1021/acsami.1c03753
ACS Appl. Mater. Interfaces 2021, 13, 28442−28450

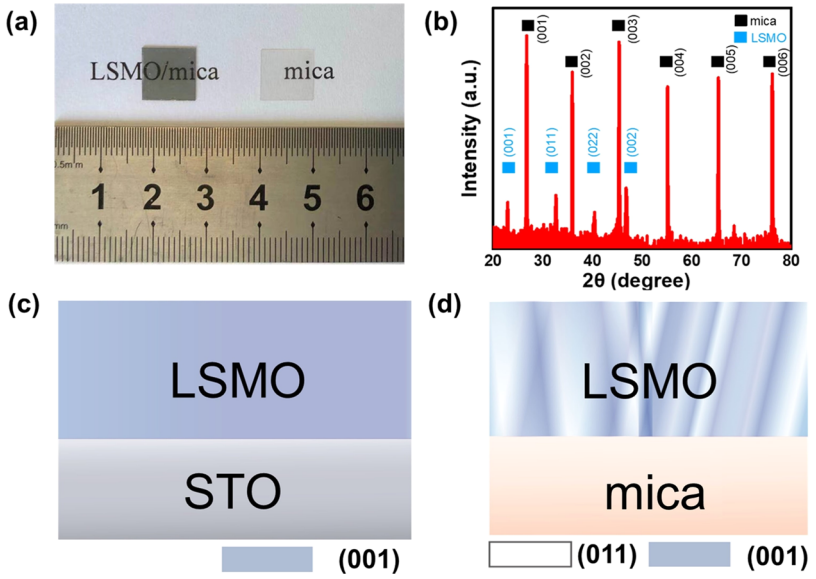

Figure 1. (a) Optical images of LSMO/mica and mica materials covering text printed on paper. The gray transparent sample on the left is the LSMO/mica heterostructure and the white transparent sample on the right is the mica substrate. (b) XRD pattern of the LSMO/mica heterostructure. Schematic diagram of (c) the epitaxial growth of LSMO(001) on the STO substrate and (d) cogrowth of LSMO(001) and LSMO(011) on the mica substrate. The LSMO(001)- and LSMO(011)-oriented columns are represented by the blue and white areas, respectively.

functional oxides, such as VO_2,[29] Fe_3O_4,[30] $BaTi_{0.95}Co_{0.05}O_3$,[31] etc.[32−35] In contrast to traditional organic flexible substrates with low melting points (generally less than 300 °C), such as poly(dimethylsiloxane) (PDMS), poly(vinylidene fluoride) (PVDF), and other polymer materials,[36−40] mica is considered one of the best natural substrate candidates for high-temperature oxide growth environments. It has been reported that LSMO films deposited on mica substrates have more GBs and a larger degree of disorder than those deposited on rigid substrates such as strontium titanate (STO) and lanthanum aluminate (LAO), which render distinct transport properties.[41] Nevertheless, the CMR effect of LSMO films deposited on mica substrates has not been fully studied. To our knowledge, no study on the LFMR effect of flexible LSMO films has been published yet, especially for a magnetic field range as small as 0.1 T.

In this work, we investigated a combination of the above two aspects, realizing flexible and large LFMR effects in free-standing LSMO films for the first time. The LSMO/mica heterostructure was first fabricated by the pulsed laser deposition (PLD) technique. The unique interfacial properties of mica, including a relatively rough surface morphology and weak van der Waals interactions between the film and substrate, were utilized to increase the degree of disorder in LSMO films, thereby enhancing the LFMR effect. Then, a simple transfer method was designed to transfer the LSMO film grown on a mica substrate to an arbitrarily flexible substrate, resulting in a free-standing LSMO film. The LSMO films exhibited good flexibility and stability under various bending conditions, as proven by *M-R* and *M-H* characterization. Compared with traditional LSMO films, the LFMR values of these free-standing LSMO films were magnified by 80 times; such values reached up to 16% when the magnetic field was smaller than 0.1 T. In addition, our LSMO films exhibited an obvious LFMR effect in the wide temperature range from 10 to 150 K. The temperature stability was effectively improved, enabling a memoresistor stable working state. The fitting result with the spin-polarized intergrain tunneling model[24] proves that this large LFMR behavior is an intrinsic phenomenon rather than an interfacial one. Using mica-assisted lift-off technology, a prototype with a stable non-volatile multivalue storage function was achieved; materials with such properties are desirable for future application in flexible spintronics and electronics.[42−44]

RESULTS AND DISCUSSION

Growth of LSMO on a Mica Substrate. A 60 nm thick LSMO thin film was deposited on a mica(001) substrate through the PLD technique. The semitransparent nature of the LSMO/mica heterostructure was confirmed by obtaining optical images of the LSMO/mica heterostructure and the mica substrate covering text printed on paper (Figure 1a); this semitransparent heterostructure may therefore be used in optical integrated devices in the future. A typical X-ray diffraction (XRD) $\theta-2\theta$ scan of the LSMO/mica heterostructure (Figure 1b) showed both LSMO(001) and LSMO(011) peaks with a series of background peaks generated by mica(00l), confirming the cogrowth of LSMO(001) and LSMO(011) polycrystalline structures in the LSMO thin film. This result was expected since no strong binding force was provided by the mica substrate. The LSMO/mica heterostructure is governed by van der Waals forces instead of covalent bonds, leading to homogeneous nucleation and relatively disordered growth of the sequentially deposited LSMO film.[29,41] Figure 1c,d shows the schematic diagrams of the LSMO(001)/STO heterostructure epitaxial growth via covalent bonds and the LSMO(001) and LSMO(011)/mica heterostructure cogrowth via van der Waals forces, respectively. Compared to single crystals grown epitaxially on STO substrates, the cogrowth pattern allows the LSMO films grown on mica to have more artificial grain boundaries, which can be used to enhance the LFMR effect of LSMO thin films.

Exfoliation Transfer Method for Fabricating Free-Standing LSMO Films. The prepared LSMO/mica heterostructure has a certain amount of flexibility, although compared with traditional flexible substrates such as 3M tape, mica still

https://doi.org/10.1021/acsami.1c03753
ACS Appl. Mater. Interfaces 2021, 13, 28442−28450

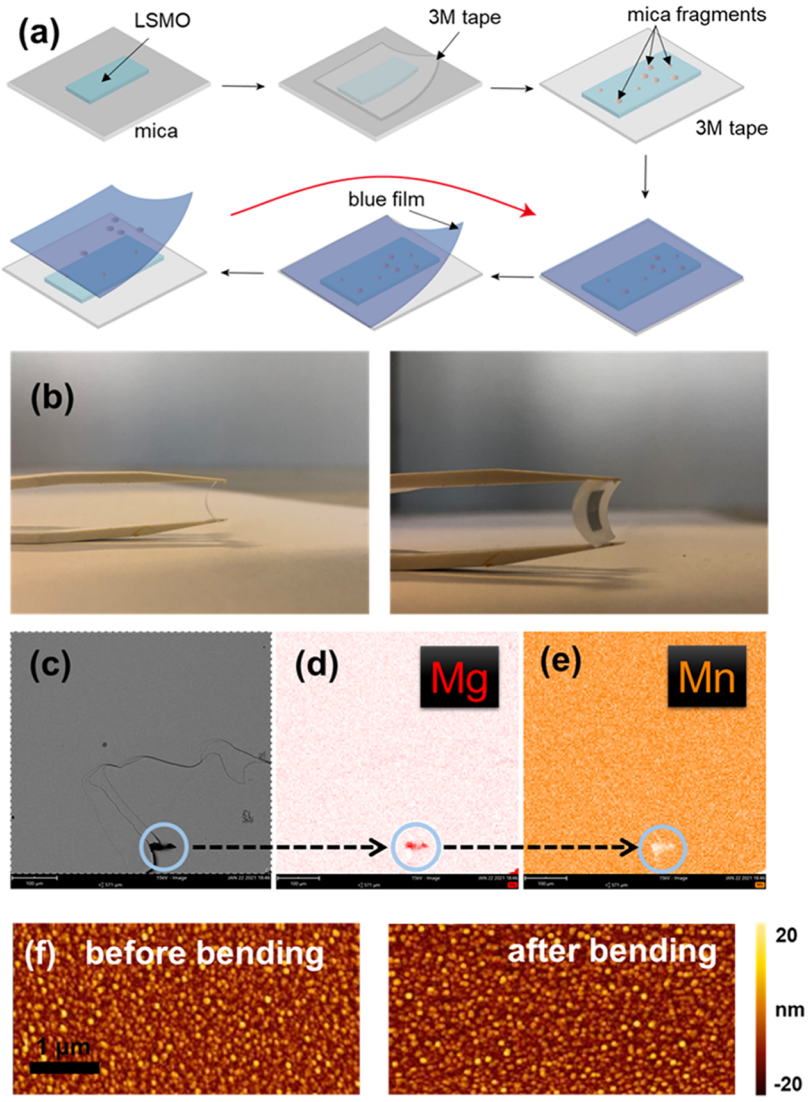

Figure 2. (a) Schematic of our exfoliation transfer method. (b) Flexibility of the free-standing LSMO sample. (c) SEM image of the free-standing LSMO film, showing no mica fragments on the LSMO surface over a considerable area. The areas inside the circles are small residual mica fragments. (d, e) EDS maps of the corresponding areas, demonstrating the distributions of (d) manganese (the characteristic element in LSMO) and (e) magnesium (the characteristic element in mica). (f) AFM surface morphologies of LSMO films before and after bending.

breaks easily under external forces. To increase the flexibility properties of LSMO films, we further developed a room-temperature exfoliation transfer method for transferring the LSMO film from the mica substrate to another more flexible substrate. Our method was inspired by the exfoliation of two-dimensional layered materials.[45,46] The fabrication process is demonstrated step-by-step in Figure 2a. In detail, we started by applying 3M tape to the top surface of the LSMO/mica heterostructure. The LSMO thin film could be easily peeled off the mica substrate due to the weak van der Waals forces between the two layers. Then, a blue protective film (NITTO SPV-KL-680) with less stickiness than the tape was used to remove the remaining mica fragments from the interface. We stamped the blue film onto the transferred LSMO film and quickly peeled it off. This process was repeated multiple times until few mica fragments were observed on the interface, finally yielding free-standing LSMO films on the 3M tape. The smooth and crack-free surface of LSMO films under the bending conditions presented in Figure 2b demonstrates the robust nature and excellent flexibility of the material. Figure 2c shows the scanning electron microscopy (SEM) image of the free-standing LSMO film with corresponding energy-dispersive spectroscopy (EDS) mapping. It is clear that there are no mica fragments on the surface of the transferred LSMO film over a considerable area, proving the effectiveness of our transfer technology. The EDS line scan information for the local area with residual mica fragments is shown in Figure S1. The surface morphology of the transferred LSMO films, as characterized by atomic force microscopy (AFM) over a measurement area of 2.5 × 5 μm, is shown in Figure 2f. The root-mean-square roughness (R_{rms}) of the film is approximately 6.19 nm. The surface morphology of the LSMO films remains unchanged (R_{rms} = 6.22 nm) after bending, indicating that the strain did not damage the microstructure of the LSMO films.[47]

Stability of Magnetic and Electronic Properties. The stability of the LSMO film upon mechanical flexing is crucial for practical applications in flexible spintronic device integration, in which the devices should maintain their original working states under bending conditions. Hence, it is necessary to systematically evaluate the magnetic and electrical stability

https://doi.org/10.1021/acsami.1c03753
ACS Appl. Mater. Interfaces 2021, 13, 28442−28450

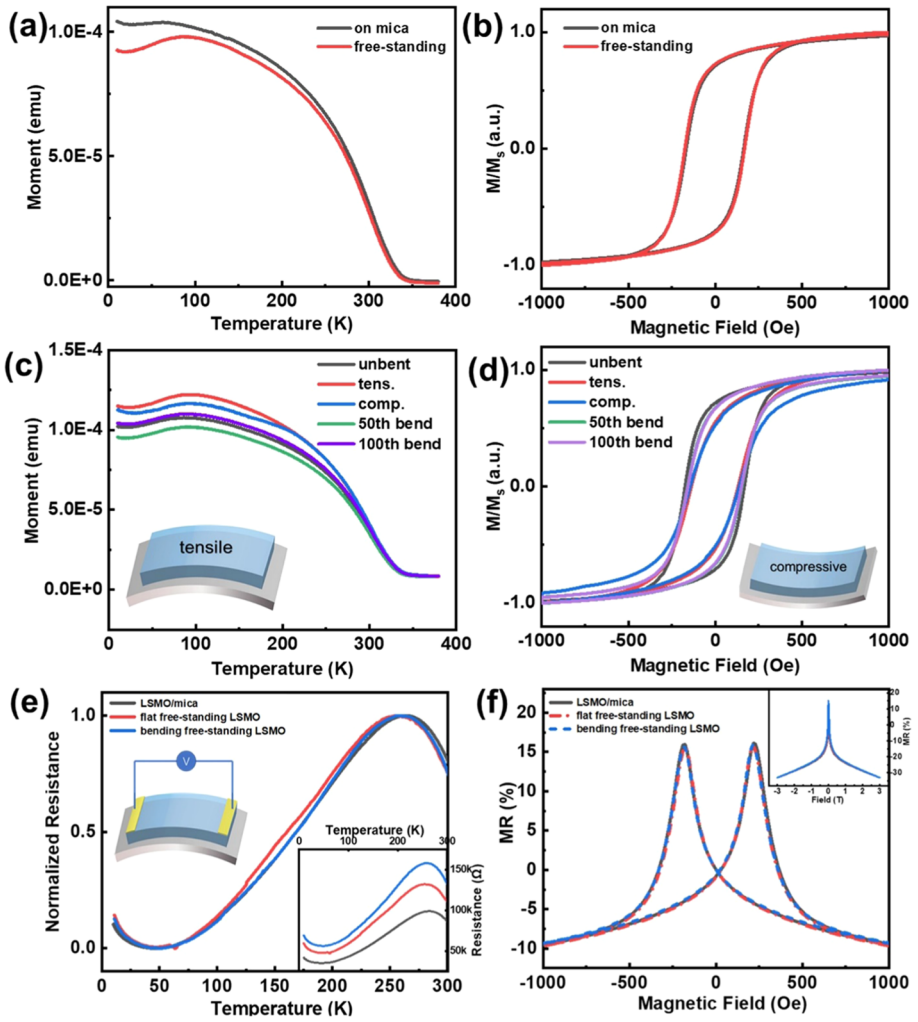

Figure 3. (a) *M-T* and (b) *M-H* curves for LSMO films before and after the exfoliation transfer process. (c) *M*−*T* and (d) *M*−*H* curves for the films under various bending conditions. (e) Normalized *R-T* curves for the three different samples; the inset shows the original *R-T* curves. (f) MR curves for the three different samples; the inset shows the high-field MR curves.

of the LSMO film. To investigate whether the quality of LSMO thin films is influenced by mechanical exfoliation, we first compared their magnetic properties before and after the transfer process. Figure 3a shows the temperature dependence of the field-cooled (FC) magnetization (*M-T*) curves for the LSMO/mica heterostructure and the transferred LSMO film at an in-plane magnetic field H = 500 Oe, where both samples exhibited almost identical trends. The magnetization increased with decreasing temperature, and a paramagnetic-to-ferromagnetic (PM-to-FM) transition was observed. The curie temperature of the LSMO/mica heterostructure (T_c = 308 K) and the free-standing LSMO film (T_c = 305 K) remained basically unchanged throughout the exfoliation transfer process. The magnetic moments of the two samples each reached their maxima at approximately 75 K and then slowly decreased during the cooling process. The normalized magnetic hysteresis loops (*M-H*) at 10 K, as recorded after field cooling from 300 K at 500 Oe, are shown in Figure 3b. Both samples presented strong ferromagnetic responses at coercivity fields (H_c) of ∼200 Oe. Similar *M-T* and *M-H* curves for the two samples indicate that our transfer technique does little harm to the LSMO film. Exploiting the relatively weak van der Waals combination forces between the film and the substrate, we successfully separated the two layers while keeping the original magnetic properties of the LSMO film basically unchanged.

The flexibility and mechanical durability of the transferred LSMO film were tested under two different bending conditions (tensile and compressive bending modes, with a curvature K = 3.72 cm^{-1}). The *M-T* and *M-H* curves remained unaltered during both compressive and tensile deformations, as shown in Figure 3c,d. It was also found that the magnetic properties of the transferred LSMO films exhibited no significant change after bending 10 000 times (Figure S2). For the electrical properties, transport measurements were conducted for a series of samples, including the LSMO/mica heterostructure, a flat transferred LSMO film, and a transferred LSMO film, under tensile bending conditions. The normalized zero-field-cooling (ZFC) temperature dependencies of the resistances showed obvious metal−insulator transitions (MITs) in all of the samples, with an almost consistent T_{MI} at approximately 256 K (Figure 3e). The resistance of the transferred LSMO film increased slightly compared to that of the LSMO/mica heterostructure, which may be ascribed to the decrease in the effective thickness of the LSMO film. In addition to the stability under bending conditions, another major advance achieved in our work was the generation of large MR effects in LSMO films, since a high on−off ratio is beneficial for the

https://doi.org/10.1021/acsami.1c03753
ACS Appl. Mater. Interfaces 2021, 13, 28442−28450

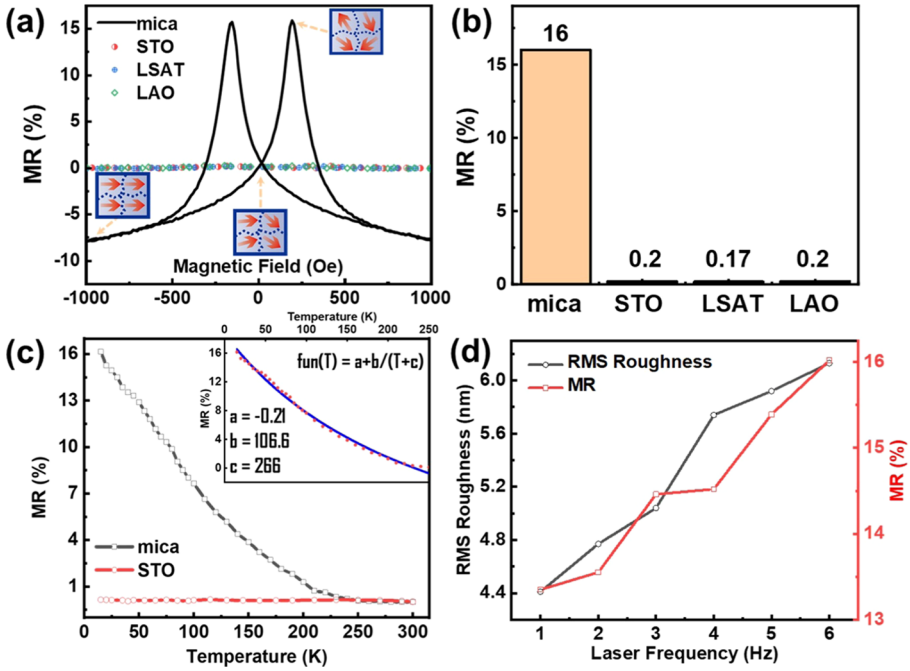

Figure 4. (a) MR curves of LSMO films on mica and other single-crystal substrates at 15 K. The blue boxes and red arrows represent the schematic LSMO films and magnetic configurations under corresponding external magnetic fields, respectively. (b) Highest MR values for different samples. (c) Temperature dependence of the maximum MR ratios in LSMO/mica and LSMO/STO heterostructures. The inset shows the relationship between temperature and the maximum MR ratio, where the red points and blue line represent the measured data and the fitted function, respectively. The fitting formula can be written as MR = $a + b / (T + c)$, where $a = -0.21$, $b = 106.6$, and $c = 266$. (d) Surface roughness and maximum MR values as a function of deposition frequency.

construction of information storaged devices. Here, MR values were defined by the equation

$$\mathrm{MR}\ (\%) = (R_H - R_0)/R_0 \times 100\%$$

R_0 and R_H are the resistivities under a zero field and a magnetic field, respectively. Figure 3f shows that the MR curves of the three samples each exhibit a consistent change pattern with a maximum MR ratio greater than 10%. Combined with the coincident normalized R-T curves, the almost overlapping MR curves prove that there is almost no difference in the electrical transport properties among the three samples.

Origin of the LFMR Effect. A large LFMR effect resulted from the polycrystalline free-standing strategy designed by us. Figure 4a shows the relationship between the MR ratio and the magnetic domain (represented by inset diagrams) as a function of the external magnetic field. The MR value of the LSMO/mica heterostructure gradually increased as the magnetic field slowly changed from −0.1 to 0.1 T, and the MR value was directly related to the magnetic degree of disorder in the films. At −0.1 T, the uniformly oriented domain structure in the LSMO films resulted in a relatively weak spin-polarized tunneling effect, which led to a smaller MR value. As the magnetic field decreased, the magnetic domain orientation became increasingly irregular, leading to a gradual increase in MR. When the magnetic field reached 190 Oe, the free-standing LSMO films transferred from mica exhibited a maximum MR value of 16% and the most disordered magnetic domain structure. This magnetic field associated with the maximum MR ratio is close to that of coercivity, indicating that the electrical transport behavior is dominated by magnetic domain rotation. Above 190 Oe, the MR value of the material gradually decreased. The MR curve showed the same pattern in reverse when the magnetic field changed. For comparison, we also measured the MR curves of epitaxial single-crystal LSMO films deposited on substrates such as STO, lanthanum aluminate-strontium aluminum tantalate (LSAT), and LAO. In particular, the MR values of these three samples were found to be less than 0.2% at low fields $B \leq 0.1$ T. The highest MR values for all samples are plotted in Figure 4b. Surprisingly, the free-standing LSMO films transferred from mica exhibited MR values 80 times larger than those of the single-crystalline films. The temperature-dependent MR values are also shown in Figure 4c. It is evident that the single-crystalline LSMO film exhibited negligible MR values from 10 to 300 K. The transferred LSMO films, however, maintained large MR values over a wide temperature range.

We believe that the large MR values for LSMO films on mica substrates over a wide range of temperatures are caused by the scattering effect, which has been enhanced at grain boundaries and vertical interfaces between LSMO(001) and LSMO(011) domains.[24,48−50] Using the spin-polarized intergrain tunneling mode proposed by Hwang et al.,[24] the temperature-dependent maximum MR ratio was well fitted, evidencing that the large LFMR in the present LSMO films originates from the intergrain tunneling (see details in Supporting Information). To further investigate the crystalline orientation-regulated mechanism, control experiments on the connections between the crystal structure, magnetic disorder, and the MR ratio were carried out. Mica has a much rougher surface (R_{rms} = 4.26 nm) than STO single-crystal substrates (R_{rms} = 0.2 nm) (Figure S3); thus, more GBs and more disordered magnetic domain structures should appear in the LSMO films grown on mica substrates. The increased number of grain and phase boundaries along with the reduced domain sizes might induce spin fluctuation and, hence, increase the MR value.[51] We measured the surface morphology of the

https://doi.org/10.1021/acsami.1c03753
ACS Appl. Mater. Interfaces 2021, 13, 28442−28450

LSMO films deposited at different frequencies on a mica substrate (Figure S4). As shown in Figure 4d, the R_{rms} surface roughness, which is related to the structural and magnetic disorder, increases with increasing growth frequency. Meanwhile, the MR value of the LSMO/mica heterostructure also increases with increasing deposition frequency. The peak MR values for LSMO films deposited at 1, 2, 3, 4, 5, and 6 Hz, as measured at H = 0.1 T, were 13.35, 13.55, 14.46, 14.52, 15.39, and 16.02%, respectively. The two curves in Figure 4d have the same trend, proving the amplification effect of spin-disordered boundaries on MR.

Realization of a Multilevel Storage Function. By utilizing the large LFMR effect, we can realize a stable, nonvolatile, multilevel storage function in free-standing LSMO films. Multistep writing (W), reading (R), and erasing (E) operations are shown in Figure 5. First, the device was turned on with a negative magnetic field of −1000 Oe, and then we reduced the magnetic field to 0 Oe, obtaining the initial state (R_0) of this device. Since the magnetic degree of disorder in the LSMO film is affected by an external magnetic field, the storage state of the device can be changed with different writing magnetic fields. The resistance signals were still remarkably distinguishable when we removed the writing magnetic fields, which means that the changes in the resistance state were nonvolatile. Taking this device as an example, we used six different magnetic fields to perform the writing operation (W_i). After removing the writing magnetic field, we read the resistance state of the device with a 1 nA current under zero field, finally obtaining six distinct sets of resistances (R_i). In addition, we erased the previously written states by applying a negative magnetic field (−1000 Oe) to the device. After the erasing process, the device was restored to the initial state (R_0) and could be used for a new round of writing/reading operations. All of the test results showed extreme stability under a low measuring current and magnetic field, indicating that this device has a great potential for application in the field of low-consumption information storage and processing.

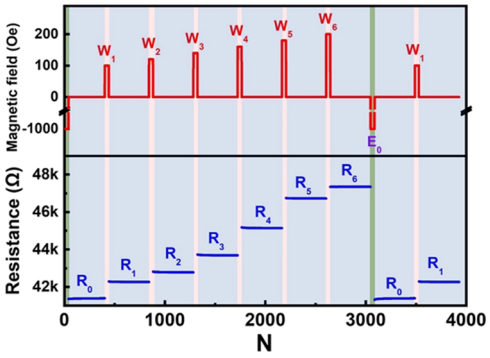

Figure 5. Write (W)−read (R)−erase (E) cycles performed on free-standing LSMO films at 10 K with a 1 nA current, where writing, reading, and erasing operations are shown via red, blue, and green areas, respectively.

CONCLUSIONS

An LSMO thin film was successfully deposited on a mica substrate through a PLD technique. Exploiting the weak van der Waals force between these two layers, we developed a room-temperature exfoliation transfer method to transfer the LSMO film from the mica substrate to another more flexible substrate, obtaining free-standing LSMO films. In addition to strong ferromagnetic and magnetoresistance properties, the transferred LSMO films also exhibited high flexibility and mechanical stability. In particular, we induced a large nonvolatile LFMR effect in the LSMO film, which was attributed to the spin-polarized intergrain tunneling effect between the grains and phases. The free-standing LSMO films transferred from mica exhibited MR values 80 times larger than those of single-crystalline films, and these large MR effects of the transferred LSMO films were maintained over a large temperature range. Taking advantage of the above characteristics, we prepared a storage prototype based on free-standing LSMO films that realized a stable, nonvolatile, and multilevel storage function. The flexibility, robustness, and large LFMR properties of free-standing LSMO films make them suitable for future flexible spintronic device applications.

EXPERIMENTAL SECTION

Thin Film Fabrication. The 60 nm LSMO films were deposited on mica(001) substrates with the pulsed laser deposition technique (KrF excimer laser, wavelength = 248 nm), using a $La_{0.7}Sr_{0.3}MnO_3$ ceramic target, which was prepared by conventional solid reaction methods. The laser beam was focused onto the target at an incidence angle of 45°, reaching an energy density of approximately 2 J/cm^2. The chamber was evacuated to a base pressure of 2×10^{-4} Pa before deposition. During deposition, the oxygen atmosphere was fixed at 50 Pa, and the temperature of the substrate was kept at 700 °C. The films were deposited at frequencies of 1, 2, 3, 4, 5, and 6 Hz. After the deposition process, the samples were cooled to room temperature at a rate of 10 °C/min in an oxygen atmosphere of 200 Pa.

Characterization and Measurement. The crystal structures of the samples were determined using a Bruker diffractometer equipped with thin-film accessories (D8 Discover, Cu Kα radiation). The surface morphology was determined using an atomic force microscope (SPI 3800N; Seiko). The scanning electron microscopy images and corresponding energy-dispersive spectroscopy mappings were collected on a Phenom ProX. Magnetic measurements were performed on a Quantum Design vibrating sample magnetometer (SQUID VSM). Resistance measurements were performed with a physical property measurement system (PPMS, Quantum Design).

ASSOCIATED CONTENT

Supporting Information

The Supporting Information is available free of charge at https://pubs.acs.org/doi/10.1021/acsami.1c03753.

EDS line information for residual mica fragments; AFM images of different substrates and heterostructures; AFM images of LSMO films deposited at different frequencies; and description and fitting parameters of the spin-polarized intergrain tunneling model (PDF)

AUTHOR INFORMATION

Corresponding Authors

Jing Wang − *Beijing National Laboratory of Condensed Matter Physics & Institute of Physics, Chinese Academy of Sciences, Beijing 100190, People's Republic of China; School of Physical Sciences, University of Chinese Academy of Sciences, Beijing 100049, People's Republic of China; Fujian Institute of Innovation, Chinese Academy of Sciences, Fuzhou, Fujian 350108, People's Republic of China;* orcid.org/0000-0001-5458-6711; Email: wangjing@iphy.ac.cn

Fengxia Hu − *Beijing National Laboratory of Condensed Matter Physics & Institute of Physics, Chinese Academy of*

https://doi.org/10.1021/acsami.1c03753
ACS Appl. Mater. Interfaces 2021, 13, 28442−28450

Sciences, Beijing 100190, People's Republic of China; School of Physical Sciences, University of Chinese Academy of Sciences, Beijing 100049, People's Republic of China; Songshan Lake Materials Laboratory, Dongguan, Guangdong 523808, People's Republic of China; orcid.org/0000-0003-0383-0213; Email: fxhu@iphy.ac.cn

Baogen Shen − *Beijing National Laboratory of Condensed Matter Physics & Institute of Physics, Chinese Academy of Sciences, Beijing 100190, People's Republic of China; School of Physical Sciences, University of Chinese Academy of Sciences, Beijing 100049, People's Republic of China; Ganjiang Innovation Academy, Chinese Academy of Sciences, Ganzhou, Jiangxi 341000, People's Republic of China;* Email: shenbg@iphy.ac.cn

Authors

Cheng Zhang − *Beijing National Laboratory of Condensed Matter Physics & Institute of Physics, Chinese Academy of Sciences, Beijing 100190, People's Republic of China; School of Physical Sciences, University of Chinese Academy of Sciences, Beijing 100049, People's Republic of China*

Shuaishuai Ding − *Tianjin Key Laboratory of Molecular Optoelectronic Sciences, Department of Chemistry, School of Sciences, Tianjin University, Tianjin 300072, People's Republic of China*

Kaiming Qiao − *Beijing National Laboratory of Condensed Matter Physics & Institute of Physics, Chinese Academy of Sciences, Beijing 100190, People's Republic of China; School of Physical Sciences, University of Chinese Academy of Sciences, Beijing 100049, People's Republic of China*

Jia Li − *Beijing National Laboratory of Condensed Matter Physics & Institute of Physics, Chinese Academy of Sciences, Beijing 100190, People's Republic of China; School of Physical Sciences, University of Chinese Academy of Sciences, Beijing 100049, People's Republic of China*

Zhe Li − *Beijing National Laboratory of Condensed Matter Physics & Institute of Physics, Chinese Academy of Sciences, Beijing 100190, People's Republic of China; School of Physical Sciences, University of Chinese Academy of Sciences, Beijing 100049, People's Republic of China*

Zhuo Yin − *Beijing National Laboratory of Condensed Matter Physics & Institute of Physics, Chinese Academy of Sciences, Beijing 100190, People's Republic of China; School of Physical Sciences, University of Chinese Academy of Sciences, Beijing 100049, People's Republic of China*

Jirong Sun − *Beijing National Laboratory of Condensed Matter Physics & Institute of Physics, Chinese Academy of Sciences, Beijing 100190, People's Republic of China; School of Physical Sciences, University of Chinese Academy of Sciences, Beijing 100049, People's Republic of China; Songshan Lake Materials Laboratory, Dongguan, Guangdong 523808, People's Republic of China*

Tongyun Zhao − *Beijing National Laboratory of Condensed Matter Physics & Institute of Physics, Chinese Academy of Sciences, Beijing 100190, People's Republic of China; Ganjiang Innovation Academy, Chinese Academy of Sciences, Ganzhou, Jiangxi 341000, People's Republic of China*

Complete contact information is available at: https://pubs.acs.org/10.1021/acsami.1c03753

Notes

The authors declare no competing financial interest.

ACKNOWLEDGMENTS

This work was supported by the National Key Research and Development Program of China (2017YFA0303601, 2019YFA0704900, 2020YFA0711502, 2018YFA0305704, 2017YFA0206300), the National Natural Sciences Foundation of China (52088101, 11934016, U1832219, 51971240, 51771223, 11921004), the Strategic Priority Research Program (B, XDB33030200), and the Key Program of the Chinese Academy of Sciences (CAS).

REFERENCES

(1) Ji, D.; Cai, S.; Paudel, T. R.; Sun, H.; Zhang, C.; Han, L.; Wei, Y.; Zang, Y.; Gu, M.; Zhang, Y.; Gao, W.; Huyan, H.; Guo, W.; Wu, D.; Gu, Z.; Tsymbal, E. Y.; Wang, P.; Nie, Y.; Pan, X. Freestanding Crystalline Oxide Perovskites Down to The Monolayer Limit. *Nature* **2019**, *570*, 87−90.

(2) Dong, G.; Li, S.; Yao, M.; Zhou, Z.; Zhang, Y.-Q.; Han, X.; Luo, Z.; Yao, J.; Peng, B.; Hu, Z.; Huang, H.; Jia, T.; Li, J.; Ren, W.; Ye, Z.-G.; Ding, X.; Sun, J.; Nan, C.-W.; Chen, L.-Q.; Li, J.; Liu, M. Super-Elastic Ferroelectric Single-Crystal Membrane with Continuous Electric Dipole Rotation. *Science* **2019**, *366*, 475−479.

(3) Guo, R.; You, L.; Lin, W.; Abdelsamie, A.; Shu, X.; Zhou, G.; Chen, S.; Liu, L.; Yan, X.; Wang, J.; Chen, J. Continuously Controllable Photoconductance in Freestanding $BiFeO_3$ By the Macroscopic Flexoelectric Effect. *Nat. Commun.* **2020**, *11*, No. 2571.

(4) Waser, R.; Aono, M. Nanoionics-Based Resistive Switching Memories. *Nat. Mater.* **2007**, *6*, 833−840.

(5) Shen, L.; Wu, L.; Sheng, Q.; Ma, C.; Zhang, Y.; Lu, L.; Ma, J.; Ma, J.; Bian, J.; Yang, Y.; Chen, A.; Lu, X.; Liu, M.; Wang, H.; Jia, C.-L. Epitaxial Lift-Off of Centimeter-Scaled Spinel Ferrite Oxide Thin Films for Flexible Electronics. *Adv. Mater.* **2017**, *29*, No. 1702411.

(6) Gu, Y.; Xu, K.; Song, C.; Zhong, X.; Zhang, H.; Mao, H.; Saleem, M. S.; Sun, J.; Liu, W.; Zhang, Z.; Pan, F.; Zhu, J. Oxygen-Valve Formed in Cobaltite-Based Heterostructures by Ionic Liquid and Ferroelectric Dual-Gating. *ACS Appl. Mater. Interfaces* **2019**, *11*, 19584−19595.

(7) Yang, W.; Shi, Q.; Miao, T.; Li, Q.; Cai, P.; Liu, H.; Lin, H.; Bai, Y.; Zhu, Y.; Yu, Y.; Deng, L.; Wang, W.; Yin, L.; Sun, D.; Zhang, X. G.; Shen, J. Achieving Large and Nonvolatile Tunable Magneto-resistance in Organic Spin Valves Using Electronic Phase Separated Manganites. *Nat. Commun.* **2019**, *10*, No. 3877.

(8) Hong, S. S.; Gu, M.; Verma, M.; Harbola, V.; Wang, B. Y.; Lu, D.; Vailionis, A.; Hikita, Y.; Pentcheva, R.; Rondinelli, J. M.; Hwang, H. Y. Extreme Tensile Strain States in $La_{0.7}Ca_{0.3}MnO_3$ Membranes. *Science* **2020**, *368*, 71−76.

(9) Pincelli, T.; Lollobrigida, V.; Borgatti, F.; Regoutz, A.; Gobaut, B.; Schlueter, C.; Lee, T. L.; Payne, D. J.; Oura, M.; Tamasaku, K.; Petrov, A. Y.; Graziosi, P.; Granozio, F. M.; Cavallini, M.; Vinai, G.; Ciprian, R.; Back, C. H.; Rossi, G.; Taguchi, M.; Daimon, H.; van der Laan, G.; Panaccione, G. Quantifying the Critical Thickness of Electron Hybridization in Spintronics Materials. *Nat. Commun.* **2017**, *8*, No. 16051.

(10) Wahler, M.; Homonnay, N.; Richter, T.; Muller, A.; Eisenschmidt, C.; Fuhrmann, B.; Schmidt, G. Inverse Spin Hall Effect in a Complex Ferromagnetic Oxide Heterostructure. *Sci. Rep.* **2016**, *6*, No. 28727.

(11) Park, J. H.; Vescovo, E.; Kim, H.-J.; Kwon, C.; Ramesh, R.; Venkatesan, T. Direct Evidence for A Half-metallic Ferromagnet. *Nature* **1998**, *392*, 794−796.

(12) Sun, D.; Fang, M.; Xu, X.; Jiang, L.; Guo, H.; Wang, Y.; Yang, W.; Yin, L.; Snijders, P. C.; Ward, T. Z.; Gai, Z.; Zhang, X. G.; Lee, H. N.; Shen, J. Active control of magnetoresistance of organic spin valves using ferroelectricity. *Nat. Commun.* **2014**, *5*, No. 4396.

(13) Ding, S.; Tian, Y.; Wang, H.; Zhou, Z.; Mi, W.; Ni, Z.; Zou, Y.; Dong, H.; Gao, H.; Zhu, D.; Hu, W. Reliable Spin Valves of Conjugated Polymer Based on Mechanically Transferrable Top Electrodes. *ACS Nano* **2018**, *12*, 12657−12664.

(14) Urushibara, A.; Moritomo, Y.; Arima, T.; Asamitsu, A.; Kido, G.; Tokura, Y. Insulator-metal Transition and Giant Magnetoresistance in $La_{1-x}Sr_xMnO_3$. *Phys. Rev. B* **1995**, *51*, 14103−14109.
(15) Takamura, Y.; Chopdekar, R. V.; Arenholz, E.; Suzuki, Y. Control of the Magnetic and Magnetotransport Properties of $La_{0.67}Sr_{0.33}MnO_3$ Thin Films through Epitaxial Strain. *Appl. Phys. Lett.* **2008**, *92*, No. 162504.
(16) Jin, S.; Tiefel, T. H.; McCormack, M.; Fastnacht, R. A.; Ramesh, R.; Chen, L. H. Thousandfold Change in rResistivity in Magnetoresistive La-Ca-Mn-O Films. *Science* **1994**, *264*, 413−415.
(17) Snyder, G. J.; Hiskes, R.; DiCarolis, S.; Beasley, M. R.; Geballe, T. H. Intrinsic Electrical Transport and Magnetic Properties of $La_{0.67}Ca_{0.33}MnO_3$ and $La_{0.67}Sr_{0.33}MnO_3$ MOCVD Thin Films and Bulk Material. *Phys. Rev. B* **1996**, *53*, 14434−14444.
(18) Fedoseev, S. A.; Pan, A. V.; Rubanov, S.; Golovchanskiy, I. A.; Shcherbakova, O. V. Large, Controllable Spikes of Magnetoresistance in $La_{2/3}Ca_{1/3}MnO_3/SrTiO_3$ Superlattices. *ACS Nano* **2013**, *7*, 286−293.
(19) Moshnyaga, V.; Damaschke, B.; Shapoval, O.; Belenchuk, A.; Faupel, J.; Lebedev, O. I.; Verbeeck, J.; van Tendeloo, G.; Mücksch, M.; Tsurkan, V.; Tidecks, R.; Samwer, K. Structural Phase Transition at the Percolation Threshold in Epitaxial $(La_{0.7}Ca_{0.3}MnO_3)_{1-x}$:$(MgO)_x$ Nanocomposite Films. *Nat. Mater.* **2003**, *2*, 247−252.
(20) Liao, Z.; Gao, P.; Stadler, S.; Jin, R.; Pan, X.; Plummer, E. W.; Zhang, J. Tuning Properties of Columnar Nanocomposite Oxides. *Appl. Phys. Lett.* **2013**, *103*, No. 043112.
(21) Kang, Y.-M.; Kim, H.-J.; Yoo, S.-I. Excellent Low Field Magnetoresistance Properties of the $La_{0.7}Sr_{0.3}Mn_{1+d}O_3^-$ Manganese Oxide Composites. *Appl. Phys. Lett.* **2009**, *95*, No. 052510.
(22) Chen, A.; Bi, Z.; Tsai, C.-F.; Lee, J.; Su, Q.; Zhang, X.; Jia, Q.; MacManus-Driscoll, J. L.; Wang, H. Tunable Low-Field Magnetoresistance in $(La_{0.7}Sr_{0.3}MnO_3)_{0.5}$:$(ZnO)_{0.5}$ Self-Assembled Vertically Aligned Nanocomposite Thin Films. *Adv. Funct. Mater.* **2011**, *21*, 2423−2429.
(23) Ning, X.; Wang, Z.; Zhang, Z. Large, Temperature-Tunable Low-Field Magnetoresistance in $La_{0.7}Sr_{0.3}MnO_3$:NiO Nanocomposite Films Modulated by Microstructures. *Adv. Funct. Mater.* **2014**, *24*, 5393−5401.
(24) Hwang, H. Y.; Cheong, S. W.; Ong, N. P.; Batlogg, B. Spin-Polarized Intergrain Tunneling in $La_{2/3}Sr_{1/3}MnO_3$. *Phys. Rev. Lett.* **1996**, *77*, 2041−2044.
(25) Levy, P.; Parisi, F.; Granja, L.; Indelicato, E.; Polla, G. Novel Dynamical Effects and Persistent Memory in Phase Separated Manganites. *Phys. Rev. Lett.* **2002**, *89*, No. 137001.
(26) Barraud, C.; Seneor, P.; Mattana, R.; Fusil, S.; Bouzehouane, K.; Deranlot, C.; Graziosi, P.; Hueso, L.; Bergenti, I.; Dediu, V.; Petroff, F.; Fert, A. Unravelling the Role of the Interface for Spin Injection into Organic Semiconductors. *Nat. Phys.* **2010**, *6*, 615−620.
(27) Li, F.; Song, C.; Cui, B.; Peng, J.; Gu, Y.; Wang, G.; Pan, F. Photon-Gated Spin Transistor. *Adv. Mater.* **2017**, *29*, No. 1604052.
(28) Cui, B.; Song, C.; Wang, G.; Yan, Y.; Peng, J.; Miao, J.; Mao, H.; Li, F.; Chen, C.; Zeng, F.; Pan, F. Reversible Ferromagnetic Phase Transition in Electrode-Gated Manganites. *Adv. Funct. Mater.* **2014**, *24*, 7233−7240.
(29) Li, C.-I.; Lin, J.-C.; Liu, H.-J.; Chu, M.-W.; Chen, H.-W.; Ma, C.-H.; Tsai, C.-Y.; Huang, H.-W.; Lin, H.-J.; Liu, H.-L.; Chiu, P.-W.; Chu, Y.-H. van der Waal Epitaxy of Flexible and Transparent VO_2 Film on Muscovite. *Chem. Mater.* **2016**, *28*, 3914−3919.
(30) Wu, P. C.; Chen, P. F.; Do, T. H.; Hsieh, Y. H.; Ma, C. H.; Ha, T. D.; Wu, K. H.; Wang, Y. J.; Li, H. B.; Chen, Y. C.; Juang, J. Y.; Yu, P.; Eng, L. M.; Chang, C. F.; Chiu, P. W.; Tjeng, L. H.; Chu, Y. H. Heteroepitaxy of Fe_3O_4/Muscovite: A New Perspective for Flexible Spintronics. *ACS Appl. Mater. Interfaces* **2016**, *8*, 33794−33801.
(31) Yang, Y.; Yuan, G.; Yan, Z.; Wang, Y.; Lu, X.; Liu, J. M. Flexible, Semitransparent, and Inorganic Resistive Memory based on $BaTi_{0.95}Co_{0.05}O_3$ Film. *Adv. Mater.* **2017**, *29*, No. 1700425.
(32) Amrillah, T.; Bitla, Y.; Shin, K.; Yang, T.; Hsieh, Y. H.; Chiou, Y. Y.; Liu, H. J.; Do, T. H.; Su, D.; Chen, Y. C.; Jen, S. U.; Chen, L. Q.; Kim, K. H.; Juang, J. Y.; Chu, Y. H. Flexible Multiferroic Bulk Heterojunction with Giant Magnetoelectric Coupling via van der Waals Epitaxy. *ACS Nano* **2017**, *11*, 6122−6130.
(33) Bitla, Y.; Chen, C.; Lee, H.-C.; Do, T. H.; Ma, C.-H.; Qui, L. V.; Huang, C.-W.; Wu, W.-W.; Chang, L.; Chiu, P.-W.; Chu, Y.-H. Oxide Heteroepitaxy for Flexible Optoelectronics. *ACS Appl. Mater. Interfaces* **2016**, *8*, 32401−32407.
(34) Liu, H.-J.; Wang, C.-K.; Su, D.; Amrillah, T.; Hsieh, Y.-H.; Wu, K.-H.; Chen, Y.-C.; Juang, J.-Y.; Eng, L. M.; Jen, S.-U.; Chu, Y.-H. Flexible Heteroepitaxy of $CoFe_2O_4$/Muscovite Bimorph with Large Magnetostriction. *ACS Appl. Mater. Interfaces* **2017**, *9*, 7297−7304.
(35) Bitla, Y.; Chu, Y.-H. van der Waals Oxide Heteroepitaxy for Soft Transparent Electronics. *Nanoscale* **2020**, *12*, 18523−18544.
(36) Wu, H.; Liu, Q.; Du, W.; Li, C.; Shi, G. Transparent Polymeric Strain Sensors for Monitoring Vital Signs and Beyond. *ACS Appl. Mater. Interfaces* **2018**, *10*, 3895−3901.
(37) Liu, G.-S.; Yang, F.; Xu, J.; Kong, Y.; Zheng, H.; Chen, L.; Chen, Y.; Wu, M. X.; Yang, B.-R.; Luo, Y.; Chen, Z. Ultrasonically Patterning Silver Nanowire−Acrylate Composite for Highly Sensitive and Transparent Strain Sensors Based on Parallel Cracks. *ACS Appl. Mater. Interfaces* **2020**, *12*, 47729−47738.
(38) Lee, Y.; Min, S.-Y.; Kim, T.-S.; Jeong, S.-H.; Won, J. Y.; Kim, H.; Xu, W.; Jeong, J. K.; Lee, T.-W. Versatile Metal Nanowiring Platform for Large-Scale Nano- and Opto-Electronic Devices. *Adv. Mater.* **2016**, *28*, 9109−9116.
(39) Zhao, D.; Chen, J.; Wang, B.; Wang, G.; Chen, Z.; Yu, J.; Guo, X.; Huang, W.; Marks, T. J.; Facchetti, A. Engineering Intrinsic Flexibility in Polycrystalline Molecular Semiconductor Films by Grain Boundary Plasticization. *J. Am. Chem. Soc.* **2020**, *142*, 5487−5492.
(40) Fukuda, K.; Yu, K.; Someya, T. The Future of Flexible Organic Solar Cells. *Adv. Energy Mater.* **2020**, *10*, No. 2000765.
(41) Huang, J.; Wang, H.; Sun, X.; Zhang, X.; Wang, H. Multifunctional $La_{0.67}Sr_{0.33}MnO_3$ (LSMO) Thin Films Integrated on Mica Substrates toward Flexible Spintronics and Electronics. *ACS Appl. Mater. Interfaces* **2018**, *10*, 42698−42705.
(42) Park, K.-I.; Son, J. H.; Hwang, G.-T.; Jeong, C. K.; Ryu, J.; Koo, M.; Choi, I.; Lee, S. H.; Byun, M.; Wang, Z. L.; Lee, K. J. Highly-Efficient, Flexible Piezoelectric PZT Thin Film Nanogenerator on Plastic Substrates. *Adv. Mater.* **2014**, *26*, 2514−2520.
(43) Gu, L.; Liu, J.; Cui, N.; Xu, Q.; Du, T.; Zhang, L.; Wang, Z.; Long, C.; Qin, Y. Enhancing the Current Density of a Piezoelectric Nanogenerator Using a Three-dimensional Intercalation Electrode. *Nat. Commun.* **2020**, *11*, No. 1030.
(44) Cheng, C.-W.; Shiu, K.-T.; Li, N.; Han, S.-J.; Shi, L.; Sadana, D. K. Epitaxial Lift-off Process for Gallium Arsenide Substrate Reuse and Flexible Electronics. *Nat. Commun.* **2013**, *4*, No. 1577.
(45) Novoselov, K. S.; Geim, A. K.; Morozov, S. V.; Jiang, D.; Zhang, Y.; Dubonos, S. V.; Grigorieva, I. V.; Firsov, A. A. Electric Field Effect in Atomically Thin Carbon Films. *Science* **2004**, *306*, 666−669.
(46) Deng, Y.; Yu, Y.; Song, Y.; Zhang, J.; Wang, N. Z.; Sun, Z.; Yi, Y.; Wu, Y. Z.; Wu, S.; Zhu, J.; Wang, J.; Chen, X. H.; Zhang, Y. Gate-tunable Room-temperature Ferromagnetism in Two-dimensional Fe_3GeTe_2. *Nature* **2018**, *563*, 94−99.
(47) Su, L.; Lu, X.; Chen, L.; Wang, Y.; Yuan, G.; Liu, J. M. Flexible, Fatigue-Free, and Large-Scale $Bi_{3.25}La_{0.75}Ti_3O_{12}$ Ferroelectric Memories. *ACS Appl. Mater. Interfaces* **2018**, *10*, 21428−21433.
(48) Rasic, D.; Sachan, R.; Temizer, N. K.; Prater, J.; Narayan, J. Oxygen Effect on the Properties of Epitaxial (110) $La_{0.7}Sr_{0.3}MnO_3$ by Defect Engineering. *ACS Appl. Mater. Interfaces* **2018**, *10*, 21001−21008.
(49) Panchal, G.; Phase, D. M.; Reddy, V. R.; Choudhary, R. J. Strain-induced Elastically Controlled Magnetic Anisotropy Switching in Epitaxial $La_{0.7}Sr_{0.3}MnO_3$ Thin Films on $BaTiO_3$ (001). *Phys. Rev. B* **2018**, *98*, No. 045417.
(50) Tsui, F.; Smoak, M. C.; Nath, T. K.; Eom, C. B. Strain-dependent Magnetic Phase Diagram of Epitaxial $La_{0.67}Sr_{0.33}MnO_3$ Thin Films. *Appl. Phys. Lett.* **2000**, *76*, 2421−2423.
(51) Köster, S. A.; Moshnyaga, V.; Samwer, K.; Lebedev, O. I.; Tendeloo, G.; Shapoval, O.; Belenchuk, A. Doping of Interfaces in

$(La_{0.7}Sr_{0.3}MnO_3)_{1-x}$:$(MgO)_x$ Composite Films. *Appl. Phys. Lett.* **2002**, *81*, 1648−1650.

https://doi.org/10.1021/acsami.1c03753
ACS Appl. Mater. Interfaces 2021, 13, 28442−28450